# Local electrochemical impedance spectroscopy: A review and some recent developments

Vicky Mei-Wen Huang, Shao-Ling Wu, Mark E. Orazem, Nadine Pébère, Bernard Tribollet, Vincent Vivier

# Local electrochemical impedance spectroscopy: A review and some recent developments

Vicky MeiWen Huang[a,1], Shao-Ling Wu[a], Mark E. Orazem[a], Nadine Pébère[b], Bernard Tribollet[c], Vincent Vivier[a,*]

[a] Department of Chemical Engineering, University of Florida, Gainesville, FL 32611, USA
[b] Université de Toulouse, CIRIMAT, UPS/INPT/CNRS, ENSIACET – 4 Allée Émile Monso, BP 44362, 31030 Toulouse Cedex 04, France
[c] LISE, UPR 15 du CNRS, Université P. et M. Curie, CP 133, 4 Place Jussieu, 75252 Paris Cedex 05, France

A B S T R A C T

Local electrochemical impedance spectroscopy (LEIS), which provides a powerful tool for exploration of electrode heterogeneity, has its roots in the development of electrochemical techniques employing scanning of microelectrodes. The historical development of local impedance spectroscopy measurements is reviewed, and guidelines are presented for implementation of LEIS. The factors which control the limiting spatial resolution of the technique are identified. The mathematical foundation for the technique is reviewed, including definitions of interfacial and local Ohmic impedances on both local and global scales. Experimental results for the reduction of ferricyanide show the correspondence between local and global impedances. Simulations for a single Faradaic reaction on a disk electrode embedded in an insulator are used to show that the Ohmic contribution, traditionally considered to be a real value, can have complex character in certain frequency ranges.

*Keywords:*
LEIS
Mathematical model
Electrode heterogeneities
Electrode kinetics
Ohmic impedance

**Contents**



## 1. Introduction

Electrochemical techniques such as cyclic voltammetry or electrochemical impedance spectroscopy (EIS) are widely used to improve the understanding of multi-step reactions [1,2], allowing the kinetics of heterogeneous electron-transfer reactions, coupled chemical reactions, or adsorption processes to be studied. In such conventional electrochemical experiments, the electrode response to a perturbation signal corresponds to a surface-averaged measurement ascribable to the behaviour of the whole electrode surface. However, electrochemical systems rarely show an ideal behaviour, and this can lead to difficulties with data interpretation. For instance, in the case of localized corrosion, surface-averaged techniques cannot identify the time of initiation or the location of a single attack among many.

To overcome these difficulties, several scanning techniques using electrodes of small dimension such as metal microelectrodes [3,4] have been developed to probe *in situ* the electrochemical

* Corresponding author.
*E-mail address:* vincent.vivier@upmc.fr (V. Vivier).
[1] Present address: Industrial Technology Research Institute, Material and Chemical Research Lab, Hsinchu 30011, Taiwan.

doi:10.1016/j.electacta.2011.03.018

interface [5]. The scanning reference electrode technique (SRET) is a rather old technique which was first introduced by Evans and Thornhill [6–8] in 1938. It consisted of measuring the potential distribution in solution with a Luggin capillary at different positions along the electrode surface, and it was successfully applied over the passing years for mapping heterogeneities during corrosion processes [9–11]. The scanning-vibrating-electrode technique (SVET), first developed for *in situ* monitoring of the steady-state current density near individual living cells by Jaffe and Nuccitelli [12], was also well-suited for studying corroding interfaces [13–17]. It is based on the use of a single microelectrode which is vibrated in one or two directions across the sample surface, allowing the potential gradient to be measured accurately with a lock-in amplifier referenced to the probe-vibration frequency [5,12]. Furthermore, the intense development of both microelectrodes and scanning electrochemical microscopy [18–22] allowed various kinds of interface to be imaged with a resolution in the micron range or lower, depending on both the electrochemical probe dimensions and the probe-to-substrate distance. In addition, various kinds of probes, such as amperometric or potentiometric sensors, can be used to selectively detect a large variety of species [23,24].

The use of local dc-current-density measurements such as SVET allows surface heterogeneities to be identified but cannot explain the local reactivity. In an attempt to evaluate the local impedance of restricted active areas, Isaacs and Kendig [25] pioneered the development of the scanning-probe impedance technique. In this technique, a small probe containing both the counter and the reference electrodes was rastered at a height of about 30 μm over the working electrode surface forming a thin-layer cell configuration. These measurements allowed qualitative results to be acquired on stainless steel welds and on coated galvanized steel plates. However, the current measured cannot be uniquely ascribable to the area under study, and, thus, no quantitative results could be obtained. Moreover, such an electrochemical-cell configuration with a small counterelectrode facing a large working electrode is not suited for impedance measurements.

A few years later, the Isaacs group introduced a novel method for generating quantitative local electrochemical impedance spectroscopy [26,27]. This technique is based on the hypothesis that the local impedance can be generated by measuring the ac-local-current density in the vicinity of the working electrode in a usual three-electrode cell configuration [26]. This was achieved with the use of a dual microelectrode for sensing the local ac-potential gradient, the local current being obtained from the direct application of the Ohm's law. It was also shown that 10 μm diameter platinum microelectrodes spaced 170 μm apart allowed a resolution of 30–40 μm, which compared favorably with the calculated results described previously for SVET experiments [15,27]. However, these authors mentioned a significant discrepancy between theory and experiments when the probe was close to the electrode under conditions when the best resolution was expected. Using this experimental setup, impedance diagrams over an active pit were obtained allowing the direct comparison of local and global impedances [28]. A variant of the technique is the mapping mode at a single frequency, which permits identification of electrochemical active areas [26–28] or time-resolved imaging for the investigation of the dynamics of the interface modifications. For instance, Wittmann et al. [29] showed that defects in organic coating can be identified by this technique prior to detection by visual observation.

Bayet et al. [30–32] developed LEIS measurements based on the use of a SVET setup. By this way, the authors took advantage of the small vibrating probe size, allowing reduction of the screening effect of the probe. They also proposed to measure the local potential in combination with the local current to define local impedance [30]. Such an approach takes advantage of using a unique probe for sensing the potential at two locations. However, one of the main drawbacks is the forced convection induced by the vibration of the probe in the close vicinity of the analyzed surface area.

Some LEIS investigations were also reported using larger probes. For instance, Baril et al. [33] investigated the electrochemical behaviour of the AZ91 magnesium alloy in $Na_2SO_4$ solution. Some local impedance diagrams were obtained over an active pit after 4 days immersion in $Na_2SO_4$ electrolyte. However, the resolution of the LEIS setup was not sufficient to describe the surface reactivity ascribable to the alloy structure of the sample. Using a home-made setup with probes of few tens of micrometers, Galicia et al. [34] were able to observe the influence of the microstructure on the corrosion rate of the AZ91 alloy. The same experimental set-up with large probes was used by Jorcin et al. [35] to investigate the initiation and propagation of delamination at the steel/organic coating interface and also by Lima-Neto [36] to determine the extension of sensitized zones in welded AISI304 stainless steel. It was shown that the length of the sensitized zone in the heat-affected zone was detected by the LEIS technique. For these two examples, industrial samples were investigated. This point is important because it emphasizes that, depending on the probe size, information can be obtained at different scales. Using a similar technique, Philippe et al. [37] investigated polymer-coated galvanized steel. They showed that the global electrochemical impedance measurements provided surface-averaged responses corresponding to both the polymer properties and its defects, whereas LEIS allowed coating defects to be isolated.

Pilaski et al. [38] developed a LEIS system based on the micro-capillary cell technique [39]. The main advantage of this technique is the possibility to investigate a small surface area independently of the surrounding material. However, this can be seen as a drawback since the effect of the surrounding material (for instance galvanic coupling) is hindered.

It should also be mentioned that the development of a specific apparatus can also be required for special applications such as fuel cell investigations [40] or for studying metal hydride battery electrodes [41]. For instance, an experimental setup allowing the simultaneous measurement of 10-local electrochemical impedance responses to be recorded in parallel has been developed for the study of a polymer electrolyte fuel cell [42,43]. A unique feature of this setup is the use of a zero resistance ammeter based on the utilization of Hall effect current sensors for the local current measurements [42]. The local impact of water and drying effects could be observed by use of the local measurements.

In a recent series of papers [44–46], our group revisited the basis of the LEIS technique. A key contribution was the definition of three local impedances. The local interfacial impedance ($z_0$) was defined to involve both a local current density and the local potential drop across the diffuse double layer. The local Ohmic impedance ($z_e$) was defined to involve a local current density and potential drop from the outer region of the diffuse double layer to the distant reference electrode. The local impedance ($z$) was thus the sum of the local interfacial impedance and the local Ohmic impedance. The influence of the cell geometry and of probe height over a disk electrode was explored theoretically [47,48]. The calculated and experimentally observed frequency dispersion and imaginary contributions to Ohmic impedance were attributed to the current and potential distributions associated with the geometry of a disk electrode embedded in an insulating plane. This work suggested that the frequency dispersion effects should not be apparent for geometries, such as a recessed electrode, for which the primary current distribution is uniform. It was also shown that low-frequency dispersion can be seen when adsorbed species are involved [49,50].

The objective of the present work is to provide guidelines for implementation of LEIS and review experimental and simulation results which are characteristic of the technique.

## 2. The LEIS setup

A fundamental requirement for the LEIS device is the measurement of the local current density in the close vicinity of the interface under investigation. Among the different possibilities presented in the introduction part, the dual probe system appears to be well suited since the fabrication of sturdy metallic microelectrodes (UME) is now well established. Furthermore, the resolution of the probe should depend, in first approximation, on both UME dimension and the inter-microelectrode distance. These two parameters can be controlled during the fabrication process.

Probes used with commercial devices are generally large and will have a limited spatial resolution (some $mm^2$). All the experimental results presented here were obtained with a home-made system. However, as stated before, the size of the probes has to be chosen in accordance with the sample dimension.

### 2.1. Electrochemical device

The experimental setup (Fig. 1) for performing LEIS measurements consisted of a home-made potentiostat coupled with a Solartron 1254 four-channel frequency response analyzer (FRA), allowing both global and local impedances to be recorded simultaneously. Two home-made analog differential amplifiers with both variable gain and high input impedance were used to record simultaneously the local potential and current variations. The local current was obtained by measuring the local potential difference sensed by the two micro probes; whereas, the local potential was measured as the potential difference between the potential of the electrode and the closest micro reference electrode. The bi-electrode was moved with a 3-axis positioning system (UTM25, Newport) driven by a motion encoder (MM4005, Newport) allowing a spatial resolution of 0.2 μm in the three directions. All measurements were generally performed under potentiostatic regulation, with the amplitude of the applied sinusoidal voltage set to be as large as possible to improve the ratio signal/noise but sufficiently low that the linear approximation of the potential/current curve can be used. For instance, some experiments have been performed using a 100 mV peak-to-peak signal, 50 acquisition cycles, and 7 points per decade of frequency [45]. Home-made software developed for scanning electrochemical microscopy was used for data acquisition. One of the great advantages of using a home-made apparatus is that it provides the capability for measuring simultaneously local and global impedances, which is not, to our best of knowledge, possible with commercial LEIS devices.

### 2.2. Probe preparation

The bi-electrode consisted of two metallic wires, the dimension of which can usually vary from few micrometers to tens of micrometers in diameter. In the case of a Pt bi-electrode, wires were sealed into the bi-capillary by melting the glass using a resistance heater with a controllable current through a coiled nichrome wire. The tip was then polished with SiC paper and a deposit of Pt black from hydrogen hexachloroplatinate (IV) was performed daily on each microdisk to reduce the interfacial impedance of these electrodes [12]. Ag/AgCl bi-microelectrodes can be constructed from silver wires sealed into a dual capillary using an epoxy resin. The AgCl layer was formed by anodizing the Ag microelectrode in a KCl solution according to the following electrochemical reaction:

$$Ag + Cl^- \rightleftarrows AgCl + e^- \tag{1}$$

The silver microelectrode was first cycled between −0.3 and 0.2 V/SCE at a rate of 100 mV $s^{-1}$ in a 2 M KCl solution for cleaning, and then a potentiostatic oxidation of Ag was performed in the same electrolyte at 0.4 V/SCE during 5–10 min. It should be mentioned that the spatial resolution can be adapted to the size of the area to be investigated by changing the size of the Ag wires used for measuring the local current and potential.

The electrochemical measurements were generally carried out with a classical three-electrode cell at room temperature. The counterelectrode was a large platinum grid, and the potentials were measured with respect to a reference electrode located far from the sample in the solution bulk as shown in the schematic representation of the experimental cell given in Fig. 1a.

## 3. Definitions of local impedances

Using a bi-electrode for probing the solution potential and a 4-channel frequency response analyzer, global, local, and local interfacial impedances can be measured simultaneously [44]. In the following, the use of an upper-case letter signifies that $Z$ is a global value; whereas, the use of a lower-case letter means that $z$ is a local value, following the notation proposed by Huang et al. [44] and summarized in the Notation section. For local electrochemical measurements, the local AC-current density $i_{loc}(\omega)$ can be obtained through the Ohm's law using

$$i_{loc}(\omega) = \frac{\Delta V_{probe}(\omega)\kappa}{d} \tag{2}$$

where $\kappa$ is the electrolyte conductivity, $\Delta V_{probe}(\omega)$ is the AC potential difference between the two probes, and $d$ is the distance between the two probes (see Fig. 1b).

The local impedance ($z$) involves the electrode potential measured with respect to a reference electrode located far from the electrode surface (Fig. 2).

$$z(\omega) = \frac{\tilde{V}(\omega) - \Phi_{ref}}{i_{loc}(\omega)} = \frac{\tilde{V}(\omega)}{\Delta V_{probe}(\omega)}\frac{d}{\kappa} \tag{3}$$

where $\tilde{V}(\omega) - \Phi_{ref}$ represents the AC potential difference between the electrode surface and the reference electrode in the bulk solution.

The local interfacial impedance ($z_0$) involves the potential of the electrode referenced to the potential of the electrolyte measured at the inner limit of the diffusion layer.

$$z_0(\omega) = \frac{\tilde{V}(\omega) - \tilde{\Phi}_0(\omega)}{i_{loc}(\omega)} = \frac{\tilde{V}(\omega) - \tilde{\Phi}_0(\omega)}{\Delta V_{probe}(\omega)}\frac{d}{\kappa} \tag{4}$$

Thus the local Ohmic impedance ($z_e$) can be deduced by calculating the difference between the local impedance and local interfacial impedance.

$$z_e(\omega) = z(\omega) - z_0(\omega) \tag{5}$$

From a practical point of view, it is not possible to perform a potential measurement just outside the double layer (Fig. 2). Thus the distance between the probe and the substrate, $h$, must be taken into account. Using the definitions presented above, the local interfacial impedance, $z_h(\omega)$, estimated at $y = h$, can be obtained using

$$z_h(\omega) = \frac{\tilde{V}(\omega) - \tilde{\Phi}_h}{i_{loc}(\omega)} = \frac{\tilde{V}(\omega) - \tilde{\Phi}_h}{\Delta V_{probe}(\omega)}\frac{d}{\kappa} \tag{6}$$

where $\tilde{V}(\omega) - \tilde{\Phi}_h$ represents the AC potential difference between the electrode surface and the closest of the two probes of the bi-electrode, located at a distance $y = h$ from the electrode surface (Figs. 1 and 2). However Eq. (6) is valid under the assumption that the spreading of the current in solution can be neglected, as previously shown by Zou and co-workers [27]. The local Ohmic impedance $z_{e,h}$ can thus be deduced by calculating the difference between the local impedance and local interfacial impedance, *i.e.*

$$z_{e,h}(\omega) = z(\omega) - z_h(\omega) \tag{7}$$

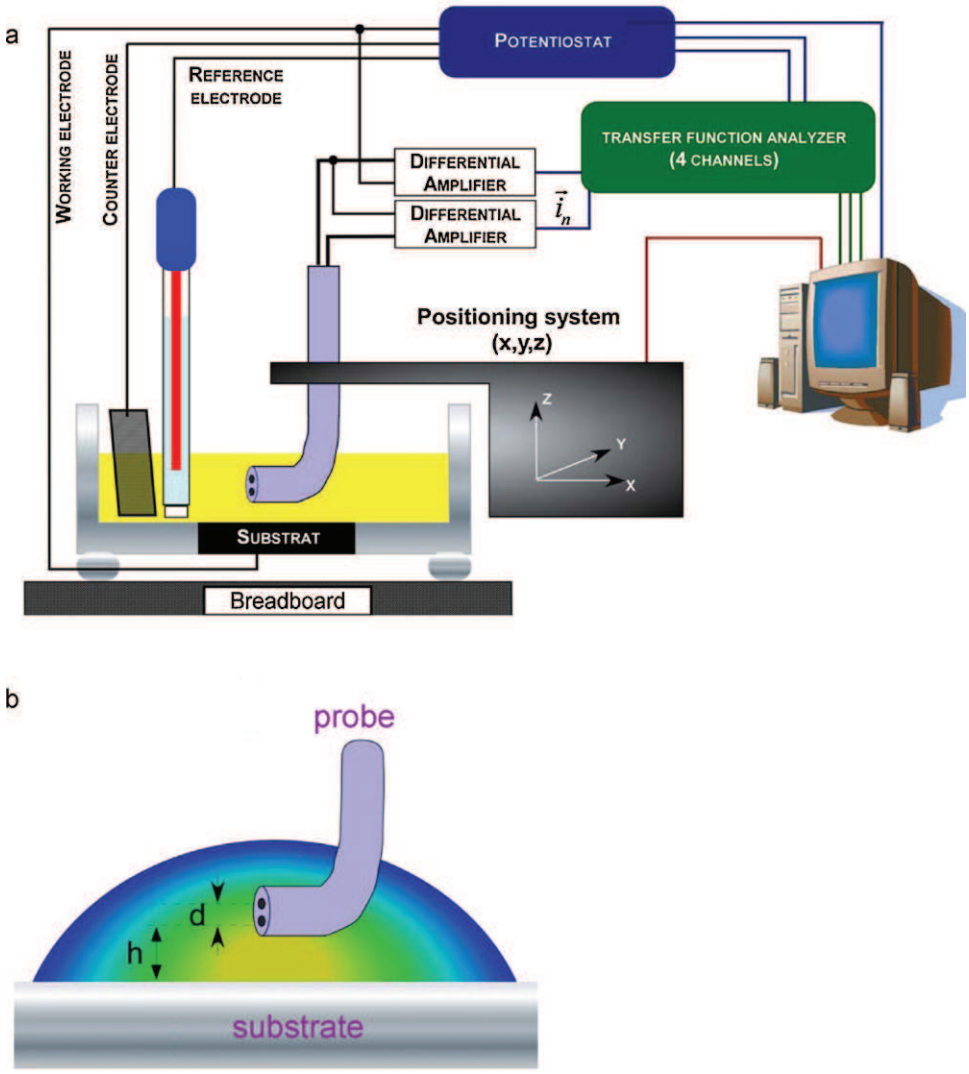


**Fig. 1.** (a) Block diagram of the LEIS setup; (b) zoom on the microprobe close to the substrate. The probe-to-sample distance is *h* and the distance between the two microreference electrodes is *d*.

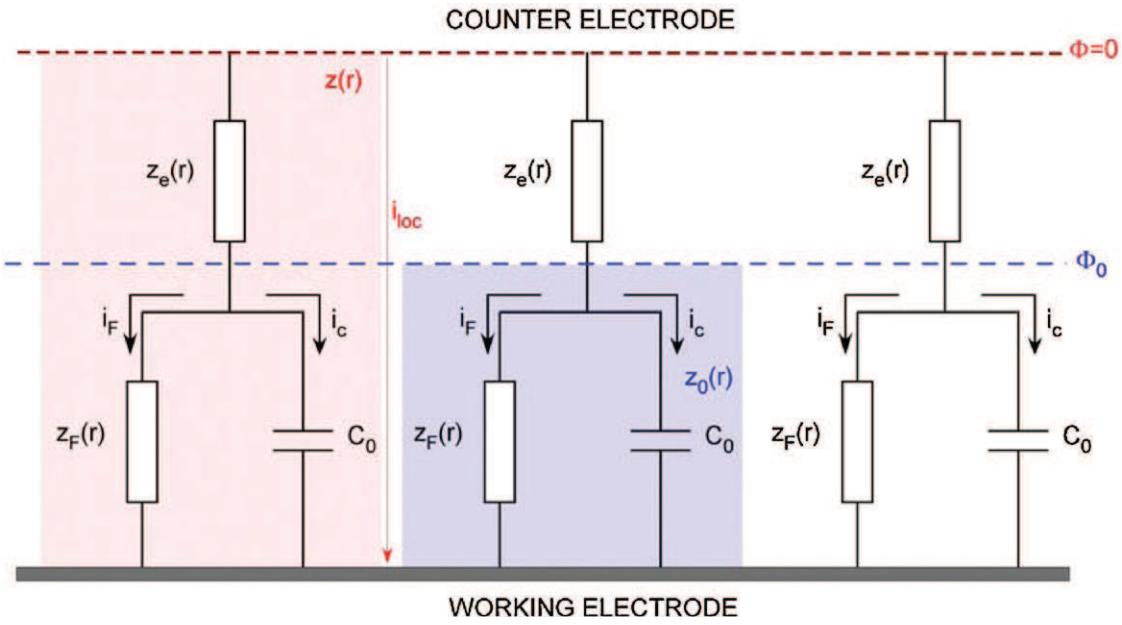


**Fig. 2.** Electrical equivalent representation of the electrochemical cell.

Experimental measurements can therefore be employed to verify the appearance of a local Ohmic impedance predicted by simulations. One can stress again that the use of home-made device for performing LEIS allowed simultaneous measurement of the global impedance and all the local impedances.

## 4. Mathematical foundation

The mathematical treatment presented by Huang et al. [44] follows that presented by Newman for a simple Faradaic reaction on a planar disk electrode embedded in a coplanar insulator [51], but it can be extended to other cell geometries [47,48] in order to investigate the edge effect of the electrode on the electrochemical impedance response, and to different mechanisms involving intermediates [49,50]. The geometry of the system was defined by the radius of the electrode $r_0$. The potential $\Phi$ in solution surrounding this electrode is governed by Laplace's equation.

$$\nabla^2 \Phi = 0 \tag{8}$$

In cylindrical coordinates ($r$,$\theta$,$y$), Eq. (8) can be expressed as

$$\frac{1}{r}\frac{\partial}{\partial r}\left(r\frac{\partial \Phi}{\partial r}\right) + \frac{1}{r^2}\frac{\partial^2 \Phi}{\partial \theta^2} + \frac{\partial^2 \Phi}{\partial y^2} = 0 \tag{9}$$

where $y$ is the normal distance to the electrode surface, $r$ is the radial coordinate, and $\theta$ is the azimuth. The cylindrical symmetry condition requires that the geometry is invariant under rotation about the $y$ axis (*i.e.* the symmetry axis), thus

$$\frac{\partial \Phi}{\partial \theta} = 0 \tag{10}$$

On the surrounding insulator and far from the electrode surface, the boundary conditions were given by

$$\left.\frac{\partial \Phi}{\partial y}\right|_{y=0} = 0 \text{ at } r > r_0 \tag{11}$$

and

$$\Phi \to 0 \text{ as } r^2 + y^2 \to \infty \tag{12}$$

For a pure capacitive behaviour, the flux boundary condition at the electrode surface was written as

$$C_0 \frac{\partial (V - \Phi_0)}{\partial t} = -\kappa \left.\frac{\partial \Phi}{\partial y}\right|_{y=0} \tag{13}$$

where $C_0$ is the interfacial capacitance, $\kappa$ is the electrolyte conductivity, $V$ is the electrode potential, and $\Phi_0$ is the potential just outside the double layer. In the case of a CPE behaviour, the governing equations were similar; the only change to be done was the substitution of the capacitance $C_0$ on the flux boundary condition of the electrode surface by $Q(j\omega)^{\alpha}$. For more complex situations, applicable boundary conditions are detailed in Refs. [46,49,50]. The current density was thus calculated by integrating the local admittance of the system over the electrode disk surface. As previously observed for a planar embedded disk electrode [44–46], the results could be expressed in terms of a dimensionless frequency, $K$, which is defined by

$$K = \frac{Q\omega^{\alpha} r_0}{\kappa} \tag{14}$$

in which $\alpha$ is taken to unity and $Q = C_0$ in the case of a pure capacitor.

For data analysis, the origin of the normal axis $y = 0$ is always defined by the disk electrode surface, that is all the distance were measured from this origin. All calculations were performed using finite element method software (COMSOL®) with the conductive media DC module in a 2D axial symmetry. The geometry and the position of the reference electrode were shown to play a significant role on the numerical result of the calculated impedance. Thus, a spherical geometry, and a distance 2000 times larger than the disk electrode dimension were used to perform numerical calculation within an error range smaller than 0.2%.

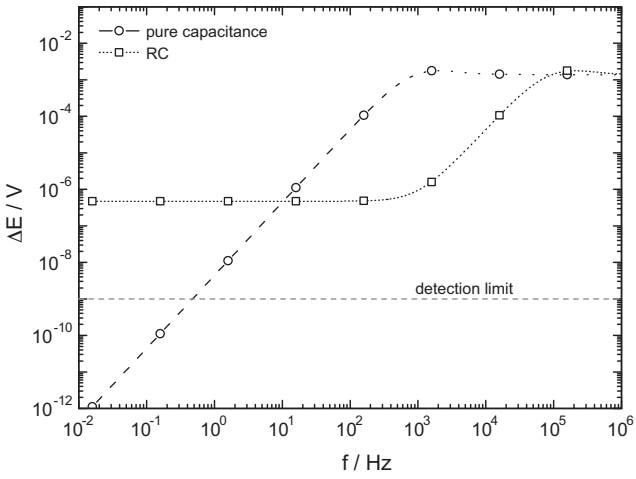


**Fig. 3.** Local potential difference measured at $h = 100\,\mu m$ with a bi-electrode ($d = 50\,\mu m$) over a planar-disk electrode. Calculations were performed for $\kappa = 0.01\,S\,cm^{-1}$; $r_0 = 0.25\,cm$; $C_0 = 10\,\mu F$; $R$ = infinity (pure capacitance—circles) and $R = 1\,k\Omega$ (squares); $\Delta V = 30\,mVpp$.

## 5. Potential difference measurement and spatial resolution

Independent of the mechanism under investigation, LEIS is based on the measurement of a local potential difference in the close vicinity of the electrochemical interface. The size of the probe and the distance between the probe and the substrate are the relevant parameters. Fig. 3 shows the local potential difference measured over a planar-disk electrode ($r_0 = 0.25\,cm$) for a probe located $h = 100\,\mu m$ of the interface with a bi-electrode (distance between the two probes, $d = 50\,\mu m$). The calculations were performed for $\kappa = 0.01\,S\,cm^{-1}$ and a double layer capacitance $C_0 = 10\,\mu F$. Two cases were considered: a blocking electrode ($R$ = infinity—circles) and $R = 1\,k\Omega$, which represents a kinetically-controlled electron-transfer reaction (squares on Fig. 3). In the case of a blocking electrode, the potential difference decreases linearly with the frequency and reaches 1 nV for 0.5 Hz. As 1 nV is a lower limit for a commercial apparatus, this is a strong limitation of the technique. However, when the system involves a single electron exchange, the curve is S-shaped and tends towards 500 nV. It should be noted that this latter value depends on both electrolyte conductivity as shown by Eq. (14) and charge-transfer resistance. As a guideline, a decrease of the electrolyte conductivity allows measurement at lower frequencies. However, if the system involves a smaller time constant, associated, for example, with diffusion or relaxation of adsorbed species, preliminary experiments are required for the determination of the lowest measurable frequency.

One approach for increasing the spatial resolution would be to decrease the probe size, but this makes sense only if the distance between the two probes also diminishes since the spatial resolution should depend on the total size of the probe. Fig. 4 shows the influence of the distance between the two microreference electrodes when the probe is located at a position 50 μm from the interface. The potential difference between the two electrodes decreases with the inter-electrode distance and reaches a value smaller than 1 nV when the probe separation is smaller than 1 μm. Fig. 5 shows that when a probe with the inter-electrode distance of 1 μm is used, the distance between the probe and the substrate does not play a significant role if $h > d$.

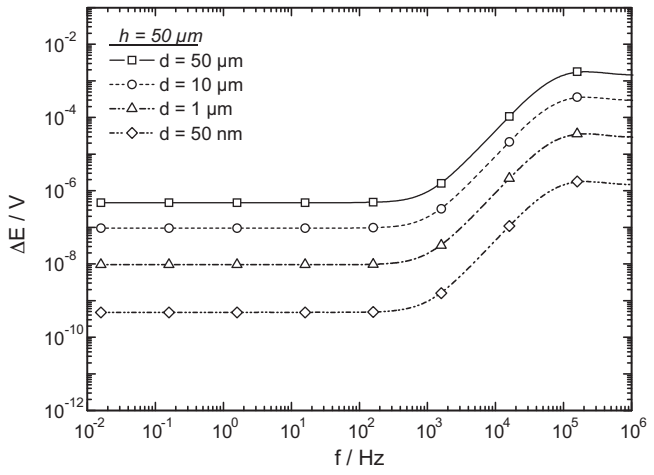


**Fig. 4.** Local potential difference measured at $h = 50\ \mu m$ over a planar-disk electrode with the distance between the two sensing electrode (d) as a parameter. Calculations were performed for $\kappa = 0.01\ S\ cm^{-1}$; $r_0 = 0.25$ cm; $C_0 = 10\ \mu F$; $R = 1\ k\Omega$; $\Delta V = 30$ mVpp.

From this series of simulations, it is shown that to increase the spatial resolution, the probe size must decrease. However, a dimension in the micrometer range or lower seems to be the actual limit. The commercial probe sizes (electrode dimension and inter-electrode distance) are significantly larger, which has the effect of decreasing the spatial resolution. However, use of larger probes allows measurement over a larger frequency domain (especially the lower frequency range).

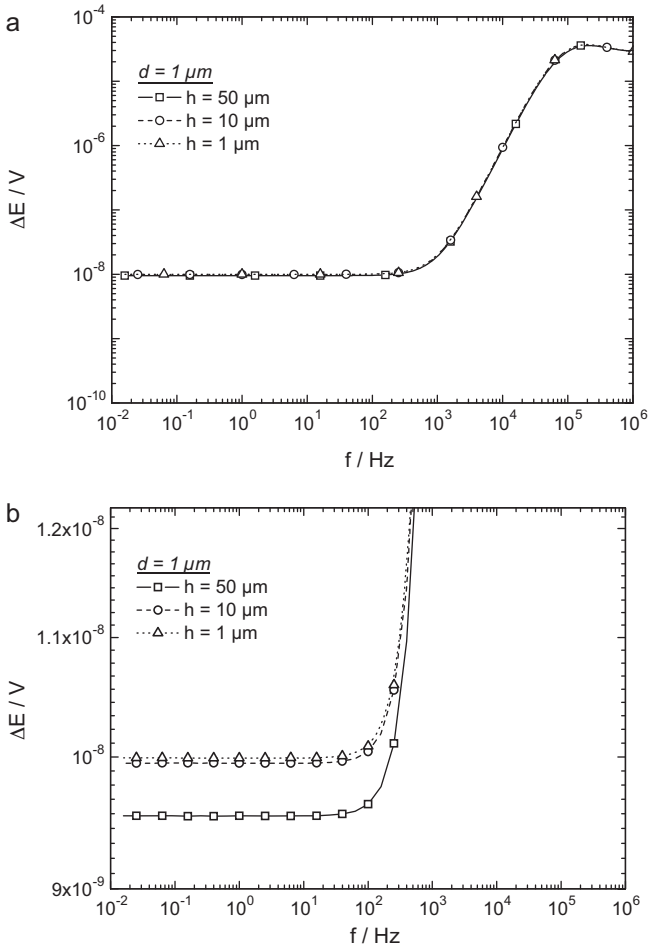


**Fig. 5.** (a) Local potential difference measured with a bi-electrode ($d = 1\ \mu m$) over a planar-disk electrode with the probe-to-substrate distance ($h$) as a parameter. Calculations were performed for $\kappa = 0.01\ S\ cm^{-1}$; $r_0 = 0.25$ cm; $C_0 = 10\ \mu F$; $R = 1\ k\Omega$; $\Delta V = 30$ mVpp. (b) Zoom on the potential difference in the low frequency range.

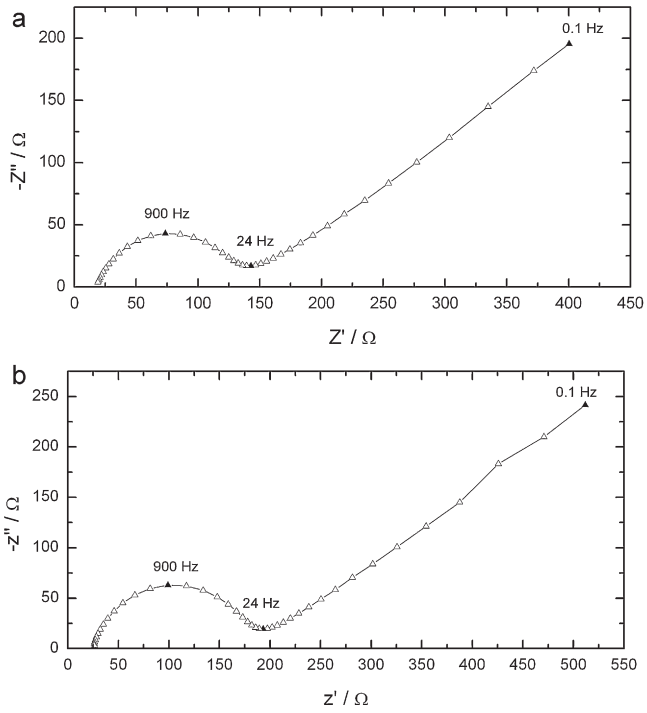


**Fig. 6.** Global (a) and local (b) impedance measurements performed simultaneously on a 0.5 cm in diameter carbon electrode in ferri-ferrocyanide solution (10 mM) + KCl (0.5 M) solution at the equilibrium potential. The local probe consisted of two 40 µm in diameter Ag/AgCl wires at 100 µm over the center of the carbon electrode.

## 6. A simple example: the ferri/ferrocyanide system

Fig. 6 shows experimental results for global and local impedance measurements performed in a ferri/ferrocyanide solution at the equilibrium potential. The bi-microelectrode which consisted of two silver/silver chloride microelectrodes of 40 µm in diameter each, was positioned at 100 µm above the carbon electrode (0.5 cm in diameter). Fig. 6a shows the global impedance. From the high-frequency loop, the electrolyte resistance, the charge transfer resistance and the double layer capacitance can be obtained. The low-frequency behaviour corresponds to the Warburg impedance (diffusion) as expected for a simple redox system at steady-state. Fig. 6b shows the local impedance diagram performed over the center of the carbon electrode, simultaneously with the global one. It is noteworthy to see that the two diagrams are identical, thus validating the local impedance measurement. In addition, the characteristic frequencies of the time constants are similar for each process. This simple experiment allows calibration of the experiment. It also shows that the same processes can be characterized with both global and local impedance spectroscopy, taking advantage of the spatial resolution of the LEIS technique. From an experimental point of view, all the requirements for performing a global impedance measurement (*i.e.* linearity, stability, and causality) remain the same for LEIS, and the validity of the measurements can be checked using the Kramers-Kronig relationship directly or through use of the measurement model [52–54].

## 7. Influence of the cell geometry on local impedance response

Huang et al. [44–46] have shown that the Ohmic contribution to the impedance response of a disk electrode embedded in an insu-

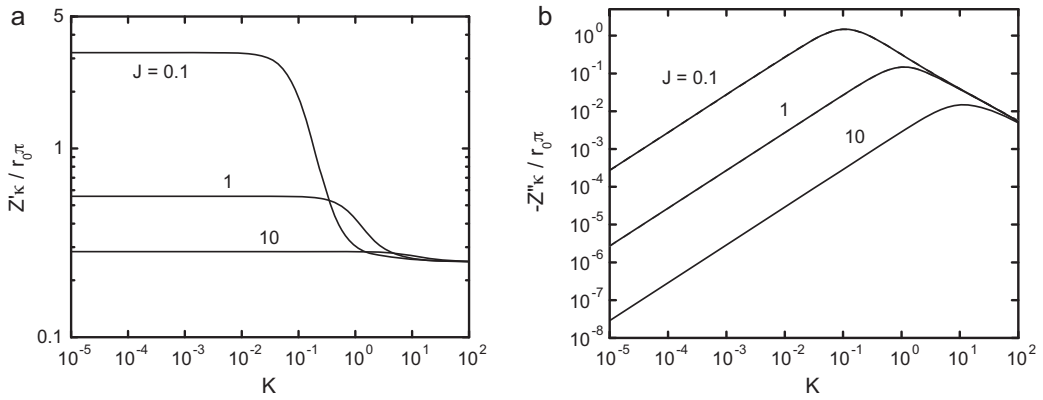


**Fig. 7.** Dimensionless impedance response for a disk electrode with a single Faradaic reaction under Tafel kinetics with $J$ as a parameter: (a) real part; and (b) imaginary part.

lating plane takes the form of an impedance. The appearance of the complex Ohmic impedance was attributed to the nonuniform current and potential distributions induced by electrode geometry. For the disk embedded in an insulating plane, the radial current density is a function of radial position and has an associated decrease in current density with axial position. In this case, the Ohmic impedance must be represented by a complex number. For the recessed disk electrode geometry, there is no radial current and the current density is independent of axial position. In this case, the Ohmic impedance can be represented by a real number. The complex character of the Ohmic impedance is therefore not only a property of electrolyte conductivity, but also a property of electrode geometry and interfacial impedance.

The simulations presented by Huang et al. [46] are extended here for a single Faradaic reaction under Tafel kinetics. The electrochemical reaction is characterized by the parameter

$$J(r) = \frac{\alpha F \left|\bar{i}(r)\right| r_0}{RT\kappa} = \frac{4}{\pi}\frac{R_e}{R_t}. \tag{15}$$

The global impedance response is presented in Fig. 7 with $J$ as a parameter. When $J$ is large, the kinetics are fast and $R_t$ is small as compared to the Ohmic resistance $R_e$. For all cases, the slope of the lines given in Fig. 7b for low frequencies is equal to unity,

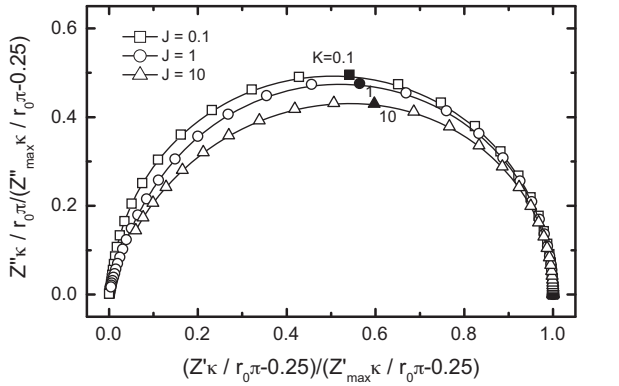


**Fig. 8.** Scaled impedance response in Nyquist format for the impedance results presented in Fig. 7.

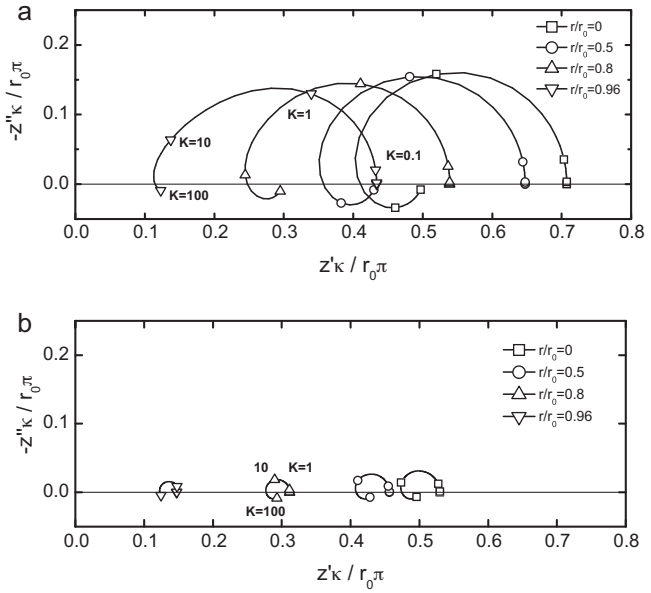


**Fig. 9.** Local impedance response for the impedance results presented in Fig. 7. (a) $J = 1$; and (b) $J = 10$.

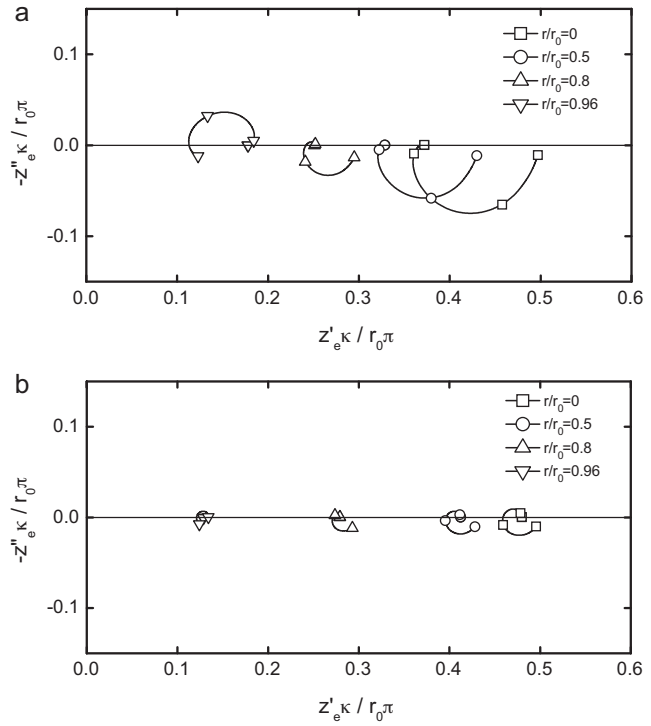


**Fig. 10.** Local Ohmic impedance response for the impedance results presented in Fig. 7. (a) $J = 1$; and (b) $J = 10$.

but the slope is greater than −1 at large frequencies. The results presented in Fig. 7 are characterized by two frequencies: $K = 1$, above which the geometry influences the impedance response and induces pseudo-CPE behaviour, and $K/J = 1$, which corresponds to the frequency $\omega = 1/R_t C_0$.

The scaled global impedance results presented in Fig. 8 shows that the influence of a large value of $J$ is to increase the appearance of a depressed semicircle usually associated with CPE behaviour. This effect is made dramatic because the characteristic frequency at which $K/J = 1$ is greater than the frequency $K = 1$.

The influence of geometry on the impedance response can be understood by examining the local impedance response shown in Fig. 9a for $J = 1$. The local impedance is largest at the center of the electrode, consistent with the smaller current density seen at the electrode center. The local impedance is smallest at the periphery of the electrode. The size of the loops is decreased in Fig. 9b for $J = 10$, consistent with the smaller value of $R_t$ relative to $R_e$. The high-frequency limit for the local impedance, however, is unchanged. The high-frequency inductive and/or capacitive loops seen in Fig. 9 are a consequence of the electrode geometry and have, in fact, been experimentally confirmed. These loops can be expressed in terms of the local Ohmic impedance discussed above.

The local Ohmic impedance for $J = 1$ and $J = 10$ is presented in Fig. 10a and b, respectively. The loops are inductive at the center of the electrode and capacitive at the electrode periphery. Again, these results have been confirmed by use of local impedance measurements. The loops associated with the local Ohmic impedance are smaller for the case where $J = 10$, which may seem to be in conflict with the result shown in Fig. 8 showing that the semicircle depression increases with increasing $J$. The reason is that, while the Ohmic impedance loops are small, they represent a larger contribution as compared to the contribution associated with the kinetics.

The frequency dependence of the local Ohmic impedance is shown in Figs. 11 and 12 for $J = 1$ and $J = 10$, respectively. At frequencies below $K = 1$, the imaginary contribution, as shown in Figs. 11b and 12b, tends toward zero. At frequencies well above $K = 1$, the imaginary contribution, again, tends toward zero. In a range of frequencies near $K = 1$, the local Ohmic contribution has a complex character. While not shown here, a similar complex character is seen for the global Ohmic contribution.

The time-constant dispersion of the global impedance response disk electrodes exhibiting geometry-induced current and potential distributions is seen for dimensionless frequency $K = \omega C_0 r_0/\kappa > 1$, which can be within the experimentally accessible range [2]. The origin of the time-constant dispersion is considered in the present work to be a complex Ohmic impedance. Blanc et al. [55] demonstrated that the concept of an Ohmic impedance is fully consistent with the pioneering calculation of frequency dispersion presented by Newman in 1970. To show that this approach is in agreement with Newman's results, they considered a blocking interface with a frequency-independent capacitance $C_0$ and an interfacial impedance $Z_0 = 1/j\omega C_0$. This interfacial impedance is independent of the electrode geometry. The overall impedance, which includes the Ohmic contribution, is $Z = Z_e + 1/j\omega C_0$, where the capacitance $C_0$ is independent of frequency and $Z_e$ is termed the Ohmic impedance. Newman, in contrast, represented the overall impedance as the sum of a frequency-dependent resistance $R_{eff}$ in series with a

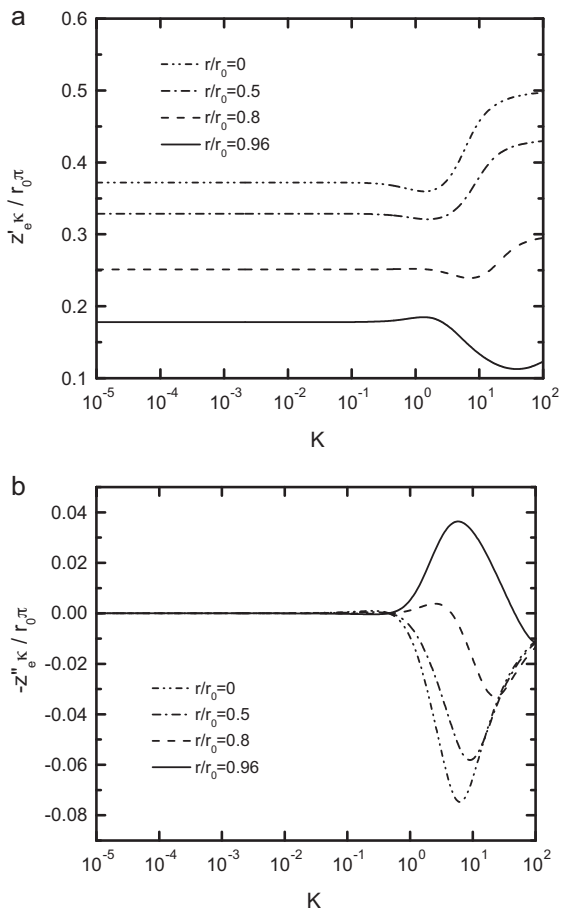


**Fig. 11.** Local Ohmic impedance response for the impedance results presented in Fig. 10a for $J = 1$: (a) real part; and (b) imaginary part.

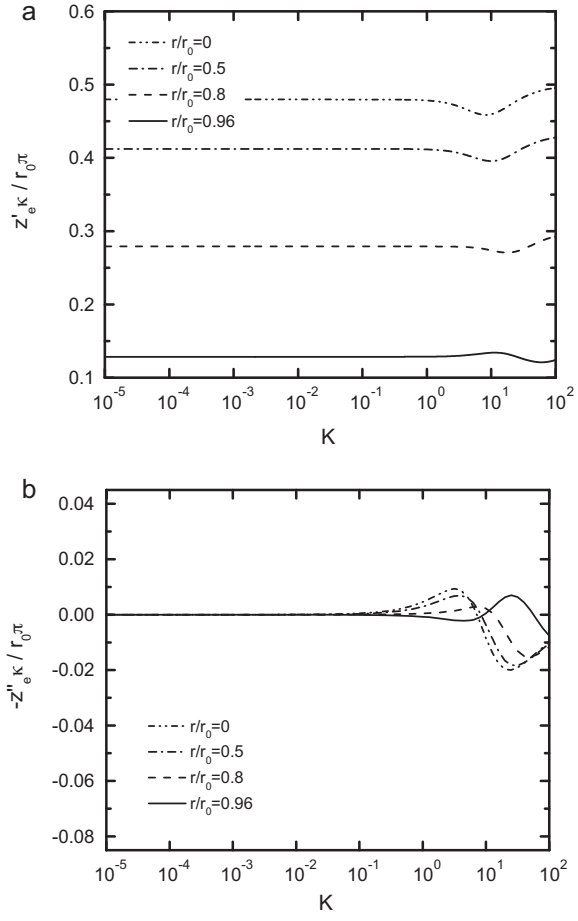


**Fig. 12.** Local Ohmic impedance response for the impedance results presented in Fig. 10b for $J = 10$: (a) real part; and (b) imaginary part.

frequency-dependent capacitance $C_{eff}$. The two descriptions of the same phenomena gives

$$Z_e + \frac{1}{j\omega C_0} = R_{eff} + \frac{1}{j\omega C_{eff}} \quad (16)$$

which yields

$$Z_e = R_{eff} - \frac{j}{\omega}\left(\frac{C_0 - C_{eff}}{C_0 C_{eff}}\right) \quad (17)$$

The fact that $Z_e$ is frequency dependent is in perfect agreement with Newman's result. When the frequency tends towards infinity, the current distribution corresponds to the primary current distribution and $\lim_{\omega\to\infty} Z_e = 1/4\kappa r_0$, in agreement with Newman's formula.

Simulations and experiments were used to show that complex Ohmic impedances could be observed at frequencies substantially lower than $K = 1$ in cases where the Faradaic reactions involved adsorbed intermediates [49,50].

## 8. Conclusions

The origin of local electrochemical impedance spectroscopy measurements can be traced back to the original development of scanning reference electrodes in 1938. The development of LEIS was motivated by the need to probe the local reactivity of heterogeneous surfaces. The power of the technique can be demonstrated by the agreement reported between experimental results and simulations. Local impedance measurements were used, for example, to confirm the appearance of a local Ohmic impedance that was predicted by simulations.

LEIS can be performed easily by measuring the local potential difference in solution, allowing the local current to be calculated. Use of a multichannel frequency response analyzer allows simultaneous measurement of global and local behaviours. The resolution of the technique depends on the size of the electrodes used in the bi-electrode probe to sense the local potential and the spacing between the electrodes. The ultimate resolution achievable is constrained by the sensitivity of the potential measuring circuitry. Measurement sensitivity on the order of 1 nV limits the resolution to the micrometer range.

Calculated and measured local and Ohmic impedances have been shown to provide insight into the frequency dispersion associated with the geometry of disk electrodes. The global impedance associated with a simple Faradaic reaction on a disk electrode is purely capacitive, but the local impedance has high-frequency inductive loops. The local impedance is influenced by the local Ohmic impedance, which has complex behaviour near dimensionless frequency $K = 1$. The imaginary part of both the local and global Ohmic impedances is equal to zero at both high and low frequencies where the Ohmic impedance has purely resistive character.

## Appendix A. Notation

| Symbol | Meaning units |
|---|---|
| $C_0$ | interfacial capacitance ($F\,cm^{-2}$) |
| $d$ | distance between the two probes (cm) |
| $h$ | distance between the probe and the sample (cm) |
| $i_{loc}$ | local ac current density ($A\,cm^2$) |
| $K$ | dimensionless frequency ($K = \omega C_0 r_0/\kappa$) |
| $r$ | radial coordinate (cm) |
| $r_0$ | electrode radius (cm) |
| $V$ | electrode potential (V) |
| $\Delta V_{probe}$ | ac potential difference between the two probes (V) |
| $y$ | axial coordinate (cm) |
| $Z$ | global impedance ($\Omega$ or $\Omega\,cm^2$) |
| $Z'$ | real part of the global impedance ($\Omega$ or $\Omega\,cm^2$) |
| $Z'$ | imaginary part of the global impedance ($\Omega$ or $\Omega\,cm^2$) |
| $z$ | local impedance ($\Omega\,cm^2$) |
| $z'$ | real part of the local impedance ($\Omega\,cm^2$) |
| $z''$ | imaginary part of the local impedance ($\Omega\,cm^2$) |
| $z_e$ | local Ohmic impedance ($\Omega\,cm^2$) |
| $z'_e$ | real part of the local Ohmic impedance ($\Omega\,cm^2$) |
| $z''_e$ | imaginary part of the local Ohmic impedance ($\Omega\,cm^2$) |
| $z_0$ | local interfacial impedance ($\Omega\,cm^2$) |
| $z'_0$ | real part of the local interfacial impedance ($\Omega\,cm^2$) |
| $z''_0$ | imaginary part of the local interfacial impedance ($\Omega\,cm^2$) |
| $z_h$ | local interfacial impedance estimated at $y = h$ ($\Omega\,cm^2$) |
| $z'_h$ | real part of the local interfacial impedance estimated at $y = h$ ($\Omega\,cm^2$) |
| $z''_h$ | imaginary part of the local interfacial impedance estimated at $y = h$ ($\Omega\,cm^2$) |
| $z_{e,h}$ | local Ohmic impedance estimated at $y = h$ ($\Omega\,cm^2$) |
| $\kappa$ | electrolyte conductivity ($\Omega^{-1}\,cm^{-1}$) |
| $\Phi_{ref}$ | potential of the reference electrode (V) |
| $\Phi_0$ | potential at the inner limit of the diffusion layer (V) |
| $\omega$ | angular frequency, $\omega = 2\pi f\,s^{-1}$ |

## References


[1] A.J. Bard, L.R. Faulkner, Electrochemical Methods: Fundamentals and Applications, 2nd ed., Wiley-VCH, New York, 2001.
[2] C. Gabrielli, in: I. Rubinstein (Ed.), Physical Electrochemistry. Principles, Methods, and Applications, Marcel Dekker, New York, 1995 (Ch. 6).
[3] R.M. Wightman, Anal. Chem. 53 (1981) 1125A.
[4] C. Amatore, in: I. Rubinstein (Ed.), Physical Electrochemistry. Principles, Methods, and Applications, Marcel Dekker, Inc., New York, 1995 (Ch. 4).
[5] R.S. Lillard, in: P. Marcus, F. Mansfeld (Eds.), Analytical Methods in Corrosion Science and Engineering, CRC Press, Boca Raton, 2006.
[6] U.R. Evans, Nature (London, United Kingdom) 142 (1938) 160.
[7] R.S. Thornhill, U.R. Evans, J. Chem. Soc. (1938) 2109.
[8] R.S. Thornhill, U.R. Evans, J. Chem. Soc. (1938) 614.
[9] H.S. Isaacs, G. Kissel, J. Electrochem. Soc. 119 (1972) 1628.
[10] J.W. Campbell, R.D. Braun, Instrum. Sci. Technol. 24 (1996) 195.
[11] N. Cui, H.Y. Ma, J.L. Luo, S. Chiovelli, Electrochem. Commun. 3 (2001) 716.
[12] L.F. Jaffe, R. Nuccitelli, J. Cell. Biol. 63 (1974) 614.
[13] M.J. Franklin, D.C. White, H.S. Isaacs, Corros. Sci. 33 (1992) 251.
[14] H.S. Isaacs, Corros. Sci. 28 (1988) 547.
[15] H.S. Isaacs, J. Electrochem. Soc. 138 (1991) 722.
[16] R. Oltra, V. Vignal, Corros. Sci. 49 (2007) 158.
[17] B. Vuillemin, X. Philippe, R. Oltra, V. Vignal, L. Coudreuse, L.C. Dufour, E. Finot, Corros. Sci. 45 (2003) 1143.
[18] A.J. Bard, F.-R.F. Fan, J. Kwak, O. Lev, Anal. Chem. 61 (1989) 132.
[19] P. Sun, F.O. Laforge, M.V. Mirkin, Phys. Chem. Chem. Phys. 9 (2007) 802.
[20] S.E. Pust, D. Scharnweber, C.N. Kirchner, G. Wittstock, Advanced Materials, 19, Weinheim, Germany, 2007, p. 878.
[21] C. Gabrielli, F. Huet, M. Keddam, P. Rousseau, V. Vivier, J. Phys. Chem. B 108 (2004) 11620.
[22] C. Gabrielli, S. Joiret, M. Keddam, H. Perrot, N. Portail, P. Rousseau, V. Vivier, J. Electrochem. Soc. 153 (2006) B68.
[23] G. Denuault, G. Nagy, K. Toth, in: A.J. Bard, M.V. Mirkin (Eds.), Scanning Electrochemical Microscopy, Marcel Dekker, Inc., New York, 2001 (Ch. 10).
[24] M. Etienne, A. Schulte, S. Mann, G. Jordan, I.D. Dietzel, W. Schuhmann, Anal. Chem. 76 (2004) 3682.
[25] H.S. Isaacs, M.W. Kendig, Corrosion (Houston, TX, United States) 36 (1980) 269.
[26] R.S. Lillard, P.J. Moran, H.S. Isaacs, J. Electrochem. Soc. 139 (1992) 1007.
[27] F. Zou, D. Thierry, H.S. Isaacs, J. Electrochem. Soc. 144 (1997) 1957.
[28] I. Annergren, D. Thierry, F. Zou, J. Electrochem. Soc. 144 (1997) 1208.
[29] M.W. Wittmann, R.B. Leggat, S.R. Taylor, J. Electrochem. Soc. 146 (1999) 4071.
[30] E. Bayet, F. Huet, M. Keddam, K. Ogle, H. Takenouti, J. Electrochem. Soc. 144 (1997) L87.
[31] E. Bayet, F. Huet, M. Keddam, K. Ogle, H. Takenouti, Mater. Sci. Forum 289–292 (1998) 57.
[32] E. Bayet, F. Huet, M. Keddam, K. Ogle, H. Takenouti, Electrochim. Acta 44 (1999) 4117.
[33] G. Baril, C. Blanc, M. Keddam, N. Pebere, J. Electrochem. Soc. 150 (2003) B488.
[34] G. Galicia, N. Pebere, B. Tribollet, V. Vivier, Corros. Sci. 51 (2009) 1789.
[35] J.B. Jorcin, E. Aragon, C. Merlatti, N. Pebere, Corros. Sci. 48 (2006) 1779.
[36] P. Lima-Neto, J.P. Farias, L.F. Herculano, H.C. de Miranda, W.S. Araujo, J.B. Jorcin, N. Pebere, Corros. Sci. 50 (2008) 1149.

[37] L.V.S. Philippe, G.W. Walter, S.B. Lyon, J. Electrochem. Soc. 150 (2003) B111.
[38] M. Pilaski, T. Hamelmann, A. Moehring, M.M. Lohrengel, Electrochim. Acta 47 (2002) 2127.
[39] H. Krawiec, V. Vignal, R. Oltra, Electrochem. Commun. 6 (2004) 655.
[40] D.J.L. Brett, S. Atkins, N.P. Brandon, V. Vesovic, N. Vasileiadis, A. Kucernak, Electrochem. Solid State Lett. 6 (2003) A63.
[41] P. Georen, A.K. Hjelm, G. Lindbergh, A. Lundqvist, J. Electrochem. Soc. 150 (2003) A234.
[42] I.A. Schneider, H. Kuhn, A. Wokaun, G.G. Scherer, J. Electrochem. Soc. 152 (2005) A2092.
[43] I.A. Schneider, D. Kramer, A. Wokaun, G.G. Scherer, Electrochem. Commun. 7 (2005) 1393.
[44] V.M.-W. Huang, V. Vivier, M.E. Orazem, N. Pebere, B. Tribollet, J. Electrochem. Soc. 154 (2007) C81.
[45] V.M.-W. Huang, V. Vivier, I. Frateur, M.E. Orazem, B. Tribollet, J. Electrochem. Soc. 154 (2007) C89.
[46] V.M.-W. Huang, V. Vivier, M.E. Orazem, N. Pebere, B. Tribollet, J. Electrochem. Soc. 154 (2007) C99.
[47] I. Frateur, V.M. Huang, M.E. Orazem, B. Tribollet, V. Vivier, J. Electrochem. Soc. 154 (2007) C719.
[48] I. Frateur, V.M.-W. Huang, M.E. Orazem, N. Pebere, B. Tribollet, V. Vivier, Electrochim. Acta 53 (2008) 7386.
[49] S.L. Wu, M.E. Orazem, B. Tribollet, V. Vivier, J. Electrochem. Soc. 159 (2009) C28.
[50] S.L. Wu, M.E. Orazem, B. Tribollet, V. Vivier, J. Electrochem. Soc. 156 (2009) C214.
[51] J. Newman, J. Electrochem. Soc. 117 (1970) 198.
[52] P. Agarwal, M.E. Orazem, L.H. Garci-Rubio, J. Electrochem. Soc. 139 (1992) 1917.
[53] P. Agarwal, M.E. Orazem, L.H. Garcia-Rubio, J. Electrochem. Soc. 142 (1995) 4159.
[54] P. Agarwal, O.D. Crisalle, M.E. Orazem, L.H. Garcia-Rubio, J. Electrochem. Soc. 142 (1995) 4149.
[55] C. Blanc, M.E. Orazem, N. Pebere, B. Tribollet, V. Vivier, S. Wu, Electrochim. Acta 55 (2010) 6313.